

Contents lists available at [ScienceDirect](#)

Journal of the Mechanics and Physics of Solids

journal homepage: www.elsevier.com/locate/jmps

Defects in flexoelectric solids



Sheng Mao, Prashant K. Purohit*

Department of Mechanical Engineering and Applied Mechanics, University of Pennsylvania, Philadelphia, PA 19104, USA

ARTICLE INFO

Article history:

Received 11 November 2014

Received in revised form

28 April 2015

Accepted 25 July 2015

Available online 29 July 2015

Keywords:

Point defects

Dislocation

Fracture

Flexoelectricity

ABSTRACT

A solid is said to be flexoelectric when it polarizes in proportion to strain gradients. Since strain gradients are large near defects, we expect the flexoelectric effect to be prominent there and decay away at distances much larger than a flexoelectric length scale. Here, we quantify this expectation by computing displacement, stress and polarization fields near defects in flexoelectric solids. For point defects we recover some well known results from strain gradient elasticity and non-local piezoelectric theories, but with different length scales in the final expressions. For edge dislocations we show that the electric potential is a maximum in the vicinity of the dislocation core. We also estimate the polarized line charge density of an edge dislocation in an isotropic flexoelectric solid which is in agreement with some measurements in ice. We perform an asymptotic analysis of the crack tip fields in flexoelectric solids and show that our results share some features from solutions in strain gradient elasticity and piezoelectricity. We also compute the energy release rate for cracks using simple crack face boundary conditions and use them in classical criteria for crack growth to make predictions. Our analysis can serve as a starting point for more sophisticated analytic and computational treatments of defects in flexoelectric solids which are gaining increasing prominence in the field of nanoscience and nanotechnology.

© 2015 Elsevier Ltd. All rights reserved.

1. Introduction

Flexoelectricity refers to the coupling of electric polarization to strain gradients. It has been studied in-depth in liquid crystals (Meyer, 1969; Harden et al., 2010; Buka and Eber, 2012) and biomembranes (Raphael et al., 2010; Petrov, 2006). However, in recent years there has been a surge in interest in flexoelectric phenomena in harder materials, such as lead zirconate titanate (PZT) and other perovskites (Nguyen et al., 2013; Zubko et al., 2013). The primary reason for this development is the advent of accurate probes that can detect polarizations and stresses at the nano-scale (Ma and Cross, 2001, 2002; Zubko et al., 2007; Catalan et al., 2011; Chin et al., 2015). Concurrent developments have also taken place in the theoretical interpretations of the experiments. Atomistic simulations, such as lattice dynamics (Maranganti and Sharma, 2009) and first principles calculation (Hong and Vanderbilt, 2011, 2013) have shed some light on the microscopic origins of flexoelectric phenomena in solids and given estimates for the magnitude of the flexoelectric constants. On the other hand, computational methods based on finite elements have been used to study stress and polarization fields in macroscopic solids (Abdollahi et al., 2014). Recently, we presented analytic solutions to some boundary value problems in flexoelectric solids in one and two dimensions (Mao and Purohit, 2014). Our goal in this paper is to utilize that framework to describe the

* Corresponding author.

E-mail address: purohit@seas.upenn.edu (P.K. Purohit).

stress and polarization fields near defects in flexoelectric solids. Defects are the spots where the effects of flexoelectricity are expected to be prominent due to the large strain gradients in their vicinity. Our analysis will enable better interpretation of experimental data since most specimens inevitably have defects in them.

Flexoelectricity also offers a simpler alternative explanation to some phenomena that have been discovered before. In the 1960s and 1970s a series of experiments (Koehler et al., 1962; Turchányi et al., 1973; Whitworth, 1975) were performed to study charged dislocations in cubic crystals, i.e. alkali halides. These solids have centrosymmetric lattices which rule out piezoelectricity as the cause for the charge carried by dislocations in them, but this symmetry does not rule out flexoelectricity. In fact, flexoelectric phenomena can be observed in dielectrics of any symmetry group, including isotropic ones. We show in this paper that some of the results for charged dislocations can be qualitatively understood in terms of flexoelectricity. Charged dislocations were also observed in experiments on ice by Petrenko and co-workers in 1980s (Petrenko and Whitworth, 1983). They conducted a thorough study of the electromechanical properties of ice and attributed charged dislocations and other phenomena to a so-called “pseudo-piezoelectricity” (Petrenko and Whitworth, 1999). This phenomenon assumed that the polarization in ice is proportional to the pressure gradient. This is a natural result of what is known today as flexoelectricity (Mao and Purohit, 2014). Indeed, Petrenko and co-workers studied point defects, dislocations and cracks in ice and arrived at their conclusions about pressure gradient dependent polarization from a microscopic view point (Petrenko, 1996). We show here that the results from our formulation based on a strain-gradient coupled polarization agree quite well with the findings of Petrenko and co-workers.

The study of cracks and other defects in closely related piezoelectric solids has a long history (Kuna, 2010). A primary motivation for these studies was to better understand damage and failure of piezoelectric devices. In particular, mathematical techniques from linear elastic fracture mechanics (LEFM) were used to find analytic solutions for a variety of crack problems in piezoelectric solids (Sosa, 1992; Suo et al., 1992; Pak, 1992) which are now referred to as linear piezoelectric fracture mechanics (LPFM). Parallel experimental studies were also conducted, as summarized in Schneider (2007). It was realized that both mechanical failure and electric breakdown are responsible for damage in piezoelectric devices due to the singular nature of the stress and electric fields near a crack tip. For example, an “electric-yielded” zone in ferroelectrics was proposed (Gao et al., 1997; Wang, 2000), which is analogous to the plastic zone in fracture mechanics. Other important developments in this field involve treatment of boundary conditions, anisotropy, mode mixing etc., as summarized in Kuna (2010). All these studies have led to the development of a powerful continuum framework to study electromechanical effects in cracks. Some insights from this literature are used in our analysis. Also, since strain gradient elasticity (SGE) is an important ingredient of flexoelectricity, we draw upon the literature on asymptotic solutions of crack tip fields in gradient elasticity (Zhang et al., 1998; Aravas and Giannakopoulos, 2009).

This paper is organized as follows. First, we construct Green’s function for a flexoelectric boundary value problem. We use it in our studies of point defects and dislocations. Second, we give an analytic solution to the problem of a single point defect in an isotropic flexoelectric solid. Third, we solve for the polarization fields of screw and edge dislocations and connect our analysis to various experiments. Fourth, we obtain asymptotic solutions to crack tip fields for Mode I and II cracks in flexoelectric solids with both conducting and insulating conditions, as well as Mode III, Mode D and Mode E cracks. We also give solutions for some mixed mode cracks. Finally, we discuss new fracture criteria that could be used for predicting failure in flexoelectric solids.

2. Flexoelectric Green’s function

We consider an isotropic flexoelectric solid in which the displacement field is $u_k(x_1, x_2, x_3)$, $k = 1, 2, 3$ and the electric potential is $\varphi(x_1, x_2, x_3)$. Such a solid is characterized by the Lamé constants, λ and μ , an SGE length scale l , two flexoelectric constants f_1 and f_2 and the dielectric permittivity ϵ . If the deformation and charge separation are sufficiently small then we can use a linearized theory and derive a Navier-type equation for the displacement field and the electric potential. The governing equations obtained in Mao and Purohit (2014) are as follows:

$$\nabla^2(a\epsilon\varphi + fu_{k,k}) = 0, \quad (1)$$

$$(\lambda + \mu)(1 - l_1^2\nabla^2)u_{k,kj} + \mu(1 - l_2^2\nabla^2)u_{j,kk} = 0, \quad (2)$$

where $\nabla^2 = \partial_{ii}$ is the Laplacian operator and l_1, l_2 and l_0 are some material length scales given by

$$l_1^2 = l^2 - \frac{\epsilon_0 f^2}{(\lambda + \mu)a\epsilon} + \frac{f_2^2}{(\lambda + \mu)a}, \quad l_2^2 = l^2 - \frac{f_2^2}{a\mu}, \quad l_0^2 = l^2 - \frac{\epsilon_0 f^2}{(\lambda + 2\mu)a\epsilon}, \quad (3)$$

with $f = f_1 + 2f_2$ and $a^{-1} = \epsilon - \epsilon_0$, where ϵ_0 is the permittivity of vacuum.

Now, let $\mathcal{L}_i = (1 - l_i^2\nabla^2)$, then the flexoelectric Green’s function for displacement G_{ij} can be obtained by solving the following equation:

$$(\lambda + \mu)\mathcal{L}_i G_{ik,kj} + \mu\mathcal{L}_2 G_{ij,kk} + \delta_{ij}\delta(\mathbf{r}) = 0, \quad (4)$$

where $\mathbf{r} = (x_1, x_2, x_3)$ is the position vector and G_{ij} corresponds to the displacement u_i in response to a unit point force in the j direction at origin. Following the techniques of Phillips (2001), we employ the Fourier transform of Green's function, \tilde{G}_{ij} . Then the equation above implies

$$(\lambda + \mu)(1 + l_1^2 q^2)q_k q_j \tilde{G}_{ik} + \mu q^2(1 + l_2^2 q^2)\tilde{G}_{ij} = \delta_{ij}. \quad (5)$$

where q_i are the coordinates in the reciprocal space and q^2 is the square sum of all q_i 's. Multiplying by q_j on each side and summing over j , we are able to solve for $q_k \tilde{G}_{ik}$:

$$q_k \tilde{G}_{ik} = \frac{q_i}{q^2(1 + l_0^2 q^2)(\lambda + 2\mu)}. \quad (6)$$

This intermediate result can be inverted to get

$$G_{ik,k} = \partial_i \left[\frac{1 - e^{-r/l_0}}{4\pi r(\lambda + 2\mu)} \right] = \frac{r_i}{4\pi r^3(\lambda + 2\mu)} \left[1 - \left(1 + \frac{r}{l_0} \right) e^{-r/l_0} \right]. \quad (7)$$

We will use this result later in our analysis of a point defect. From (5) and (6), we solve for \tilde{G}_{ij} to get

$$\tilde{G}_{ij} = \frac{\delta_{ij}}{\mu q^2(1 + l_2^2 q^2)} - \frac{q_i q_j}{q^4} \left[\frac{1}{\mu(1 + l_2^2 q^2)} - \frac{1}{(\lambda + 2\mu)(1 + l_0^2 q^2)} \right]. \quad (8)$$

We observe that due to flexoelectricity, $l_0 \neq l_2$. So, unlike in SGE, we have two different material length scales in the problem. By inverting (8) we get

$$G_{ij} = \frac{1 - e^{-r/l_2}}{4\pi\mu r} \delta_{ij} - \partial_i \partial_j \left[\frac{F_2(r)}{8\pi\mu} - \frac{F_0(r)}{8\pi(\lambda + 2\mu)} \right], \quad (9)$$

where the F_k 's are

$$F_k(r) = r + \frac{2l_k^2}{r} (1 - e^{-r/l_k}), \quad k = 0, 2. \quad (10)$$

On the other hand, the 2D Green's function is given by

$$G_{ij} = -\frac{\ln r + K_0(r/l_2)}{2\pi\mu} \delta_{ij} + \partial_i \partial_j \left[\frac{F_2(r)}{8\pi\mu} - \frac{F_0(r)}{8\pi(\lambda + 2\mu)} \right], \quad (11)$$

where the F_k 's are given by

$$F_k(r) = r^2(\ln r - 1) + 4l_k^2[\ln r + K_0(r/l_k)], \quad k = 0, 2, \quad (12)$$

and $K_0(x)$ is a modified Bessel function of the second kind. In both expressions we see the appearance of two distinct flexoelectric length scales. In the next section we will use the 3D Green's function to compute the displacement field and potential near a point defect in a flexoelectric solid.

Green's function calculated above is the solution to a point force exerted at the origin in a flexoelectric solid. To work out the solution for φ and u_i when a point charge is placed at the origin in a flexoelectric solid, the governing equation (1) must be modified to

$$\nabla^2(\varphi + \frac{f}{ae} u_{k,k}) = \frac{\rho^e}{\epsilon}, \quad (13)$$

where ρ^e is the free charge density. As a consequence, the Navier equation (2) must also be modified as

$$(\lambda + \mu)(1 - l_1^2 \nabla^2) u_{k,kj} + \mu(1 - l_2^2 \nabla^2) u_{j,kk} = \frac{f}{a} \rho_j^e, \quad (14)$$

which effectively creates a body force due to the free charge. Now, for a unit point charge, or to compute Green's function, we set $\rho^e = \delta(\mathbf{r})$. By the same technique as we used for Green's function for a point force, we find that $u_{k,k}$ is given by

$$u_{k,k} = \frac{f}{4\pi a(\lambda + 2\mu)l_0^2} \frac{\exp(-r/l_0)}{r}. \quad (15)$$

This is the flexoelectric contribution to the potential φ . By plugging the above into the electric governing equation and inverting it we get

$$G_\varphi(r) = \frac{1}{4\pi\epsilon r} \left[1 - \frac{f^2}{a^2\epsilon(\lambda + 2\mu)l_0^2} \exp\left(-\frac{r}{l_0}\right) \right]. \quad (16)$$

Clearly, we recover the classical electrostatic solution of a unit point charge in a dielectric when we let the flexoelectric

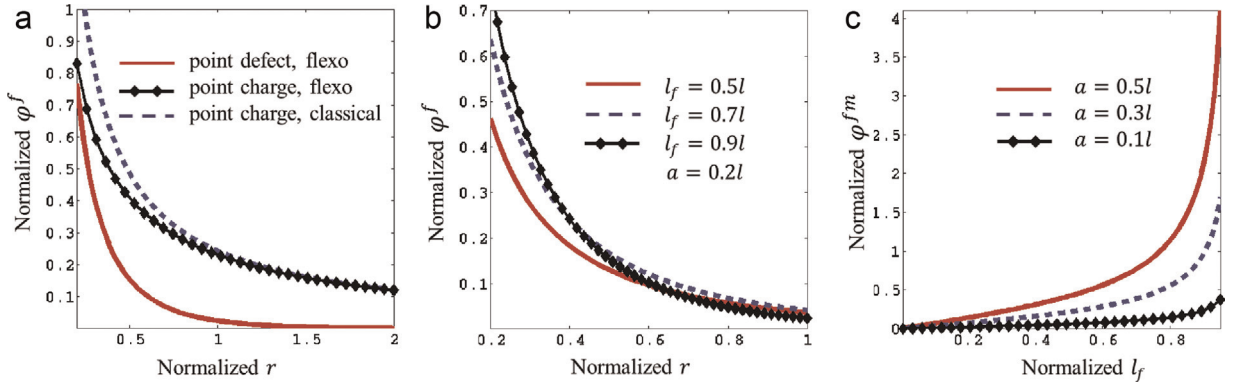


Fig. 1. In the plots above the potential is normalized against $\sqrt{(\lambda + 2\mu)l^2/\epsilon_0}$ and r is normalized against l , the SGE length scale. $l_f = \epsilon_0 f^2 / (\lambda + 2\mu)$ is the associated flexoelectric length scale. (a) depicts the difference between the potential field due to a point defect in a flexoelectric solid and that due to a point charge in a dielectric with the same dielectric constant with and without flexoelectricity. The defect curve decays rapidly. In the far field, point charge solutions converge. (b) shows how the flexoelectric constant f changes the potential field. We observe that the potential becomes negligibly small just a few diameters away from the defect. (c) shows the magnitude of the potential for various values of a , the radius of the point defect, as a function of the flexoelectric length scale l_f . We normalize l_f against l . We see that flexoelectricity is prominent only when both defect size a and l_f are comparable to l .

constant f vanish. The above solution suggests that the flexoelectric contribution to the potential is of the Yukawa type. We will see this again in the analysis of a point defect. Essentially in the far field, the potential of point charge in a flexoelectric solid and a pure dielectric converge. We illustrate this in Fig. 1.

3. Point defects

From the continuum perspective a point defect can be modeled as a spherical hole of some radius a_0 , with prescribed radial displacement δ on the surface of that hole. Following the argument of Phillips (2001), the displacement field of an isotropic point defect can be computed using Green's function as

$$u_i = -f_0 a_0 G_{ijj} = -\frac{f_0 a_0}{4\pi r^2 (\lambda + 2\mu)} \left[1 - \left(1 + \frac{r}{l_0} \right) e^{-r/l_0} \right], \quad (17)$$

where f_0 is a constant that is yet to be determined. From the boundary condition at the surface of the hole, $u_r(a_0) = \delta$, we obtain

$$u_r(r) = \frac{\delta a_0^2}{r^2} \left[\frac{1 - (1 + \gamma) e^{-\gamma}}{1 - (1 + \gamma_0) e^{-\gamma_0}} \right], \quad (18)$$

where $\gamma = r/l_0$ and $\gamma_0 = a_0/l_0$. In the limit of $a_0 \gg l_0$, we recover the elastic result (Phillips, 2001). A similar expression was obtained by Adler (1969) in the 1960s in an SGE calculation. Our result differs from that result only by a change of length scale (l_0 instead of l). Hence, in the limiting case of no flexoelectricity, our results converge to that of SGE. Intriguingly, Eringen (1984) arrived at a very similar expression for the displacement field around a point defect in a non-local piezo-electric solid. In the isotropic case his result differs from our's only by a pre-factor (a different boundary condition was used in Eringen, 1984). Note, however, that an isotropic solid cannot be piezo-electric. Hence, our result establishes an interesting connection between flexoelectricity and a non-local theory of electromechanics. This is by no means surprising since similar connections between gradient elasticity and the non-local elasticity theories are well-known (Yang, 2005).

We are interested in the variation of the electric quantities around this point defect. From Eq. (1) we can compute the potential due to its presence in an isotropic flexoelectric solid:

$$\varphi^f = -\frac{\delta a_0^2 f}{a \epsilon l_0^3 A_0} \left(\frac{e^{-\gamma}}{\gamma} \right) = -\varphi^{fm} \left(\frac{e^{-\gamma}}{\gamma} \right), \quad (19)$$

where $A_0 = 1 - (1 + \gamma_0) e^{-\gamma_0}$ and $\varphi^f \sim e^{-\gamma}/\gamma$ is a Yukawa-type potential. This result was also reported in Eringen (1984). In that work the length scale that appeared in the expressions was interpreted as the Debye screening length, which was expected to shorten due to the presence of non-local piezoelectricity. In our case the length scale appearing in the expressions has its origins in SGE and flexoelectric effects. Since here we have $l_0 < l$, flexoelectricity shortens the SGE length scale. We have plotted the potential around a point defect as a function of distance in Fig. 1(a). For comparison we have also plotted the potential field due to a point charge in a solid with the same dielectric constant as our flexoelectric solid. The field in the flexoelectric solid decays much faster. The effects of the flexoelectric length scale l_f and the defect size a_0 are analyzed in Fig. 1(b) and (c) respectively. We find that the flexoelectric effect is prominent only when l_f and a_0 are both comparable to

the SGE length scale l .

We can also work out the radial component of the polarization around our point defect:

$$P_r = \frac{\epsilon_0 \varphi^{jm}}{l_0} \left[\frac{(1 + \gamma)e^{-\gamma}}{\gamma^2} \right]. \quad (20)$$

Note that this potential and polarization field arises around a point defect even in an isotropic solid. This is because flexoelectricity arises in any dielectric irrespective of lattice symmetry. In fact, electric polarization has been detected around defects in ice (Evtushenko et al., 1987) in a pursuit for the origins of electromagnetic radiation from glaciers. In a series of experimental and theoretical works by Petrenko and co-workers this radiation was attributed to “pseudo-piezoelectricity”, in which a material had induced electric fields in proportion to pressure gradients – which is exactly (1). Petrenko et al. investigated the microscopic origins of this effect and showed that the potential field around static dislocations and cracks in ice could be consistently explained beginning with this idea (Petrenko, 1996). This idea was further employed to quantify the stress and potential fields around moving/growing cracks. That leads to the possibility of electromagnetic radiation since a time dependent pressure gradient generates a time dependent electric field (Petrenko, 1996). We will come back to this point when we analyze cracks.

Finally, with the advent of 2D flexoelectric materials, such as graphene, carbon nitride and many others, it is now possible to study the polarization field around the defects in them (Zelisko et al., 2014). The polarization fields in this case must be computed using the 2D Green's functions that we discussed in the previous section. This could be a way to validate the analytic solutions presented in this paper and others.

4. Line defects

4.1. Screw dislocation

We showed in Mao and Purohit (2014) that even though torsion of an isotropic circular rod produces a strain gradient, it does not polarize the rod due to the symmetry of the flexoelectric tensor f_{ijkl} . A similar result also holds for a material with cubic symmetry which has three flexoelectric constants. We show here that the result can be extended to screw dislocations in such materials. If the axis of the screw dislocation is along the \mathbf{e}_3 direction then the only non-zero displacement field is u_3 . Hence, the field equations for an isotropic flexoelectric solid reduce to

$$(1 - l_2^2 \nabla^2) \nabla^2 u_3 = 0, \quad \nabla^2 \varphi = 0. \quad (21)$$

These equations are the same as those in the SGE problems studied by Lazar (2013), except for a different length scale. Hence, we can directly use his results. The relevant 2D Green's function is

$$G_{33} = -\frac{1}{2\pi\mu} \left[\ln r + K_0\left(\frac{r}{l_2}\right) \right], \quad (22)$$

where $r = \sqrt{x^2 + y^2}$ and $K_0(x)$ is a modified Bessel function of the second kind. According to Lazar (2013), the distortion of a screw dislocation with a Burgers vector $(0, 0, b_z)$ can be constructed as

$$\beta_{zx} = G_{33,2} = -\frac{b_z y}{2\pi r^2} \left[1 - \frac{r}{l_2} K_1\left(\frac{r}{l_2}\right) \right], \quad (23)$$

$$\beta_{zy} = -G_{33,1} = \frac{b_z x}{2\pi r^2} \left[1 - \frac{r}{l_2} K_1\left(\frac{r}{l_2}\right) \right], \quad (24)$$

where $K_1(x)$ is a modified Bessel function of the second kind. By changing to cylindrical coordinates we get

$$\beta_{z\theta} = \frac{b_z}{2\pi r} \left[1 - \frac{r}{l_2} K_1\left(\frac{r}{l_2}\right) \right], \quad \beta_{zr} = 0, \quad (25)$$

where $\theta = \tan^{-1} y/x$. Therefore, strain \mathbf{S} can be written as $\mathbf{S} = \text{sym}\boldsymbol{\beta} = f(r)(\mathbf{e}_\theta \otimes \mathbf{e}_z + \mathbf{e}_z \otimes \mathbf{e}_\theta)$. In other words, the θ component of strain is a function of only r while all other components vanish. According to Sharma and Ganti (2005), we know

$$\nabla \otimes \mathbf{S} = f'(r)(\mathbf{e}_\theta \otimes \mathbf{e}_z + \mathbf{e}_z \otimes \mathbf{e}_\theta) \otimes \mathbf{e}_r - \frac{f(r)}{r}(\mathbf{e}_r \otimes \mathbf{e}_z + \mathbf{e}_z \otimes \mathbf{e}_r) \otimes \mathbf{e}_\theta. \quad (26)$$

These non-vanishing gradient terms do not induce any polarization in the isotropic flexoelectric solid due to the symmetry of the isotropic f_{ijkl} (no terms of the above have any repeated index). The same holds for cubic materials (Mao and Purohit, 2014). This result is consistent with Koehler et al. (1962), Turchányi et al. (1973), and Whitworth (1975), which revealed that in cubic ionic structures edge dislocations carry a charge but screw dislocations do not. We consider edge dislocations in the following section.

4.2. Edge dislocation

In the case of the edge dislocation one could follow Lazar (2013) to construct the displacement field using Green's function. However, following Eshelby (1966), we find it more convenient to work with the divergence θ and rotation Ω , which are defined as

$$\theta = u_{i,i}, \quad \Omega_i = \frac{1}{2} e_{ijk} \partial_j u_k, \quad (27)$$

where e_{ijk} is the permutation symbol. The displacement field can be reconstructed through the following equation:

$$\nabla^2 u_i = \theta_{,i} + e_{ijk} \Omega_{j,k}. \quad (28)$$

This is just the Helmholtz decomposition of $\nabla^2 u_i$, which splits it into a rotation-free part $\theta_{,i}$ and a divergence free part $e_{ijk} \Omega_{j,k}$. In this problem $\Omega = \Omega_3 = \Omega$ can be treated as a scalar. Eshelby (1966) used this idea to solve elasticity problems. In linear elasticity, θ^0 and Ω^0 are governed by the following equations:

$$\frac{\partial(\sigma\theta^0)}{\partial r} = \frac{1}{r} \frac{\partial\Omega^0}{\partial\theta}, \quad \frac{1}{r} \frac{\partial(\sigma\theta^0)}{\partial\theta} = -\frac{\partial\Omega^0}{\partial r}, \quad (29)$$

where $\sigma = (1 - \nu)/(1 - 2\nu)$ is a material constant. This means that $\sigma\theta^0$ and Ω^0 are harmonic conjugates. Now, in our problem with the isotropic flexoelectric solid, dilatation and rotation are each governed by a distinct length scale:

$$(\sigma\mathcal{L}_0\theta)_j + e_{j3k} \mathcal{L}_2\Omega_{,k} = 0, \quad j, k = 1, 2, \quad (30)$$

where $\mathcal{L}_0 = (1 - l_0^2 \nabla^2)$ and $\mathcal{L}_2 = (1 - l_2^2 \nabla^2)$ are linear operators. More explicitly, in polar coordinates:

$$\frac{\partial(\sigma\mathcal{L}_0\theta)}{\partial r} - \frac{1}{r} \frac{\partial(\mathcal{L}_2\Omega)}{\partial\theta} = 0, \quad (31)$$

$$\frac{1}{r} \frac{\partial(\sigma\mathcal{L}_0\theta)}{\partial\theta} + \frac{\partial(\mathcal{L}_2\Omega)}{\partial r} = 0. \quad (32)$$

Therefore, if we replace $\mathcal{L}_0\theta$ and $\mathcal{L}_2\Omega$ with Ω^0 and θ^0 , we recover (29). As a consequence, a solution of our problem can be constructed by solving

$$\mathcal{L}_0\theta = \theta^0, \quad \mathcal{L}_2\Omega = \Omega^0. \quad (33)$$

The solution for θ and Ω can be obtained by inverting the operators \mathcal{L}_0 and \mathcal{L}_2 . Now, suppose we have an edge dislocation with burgers vector $(b_x, 0, 0)$, then the well known elasticity solution is given by

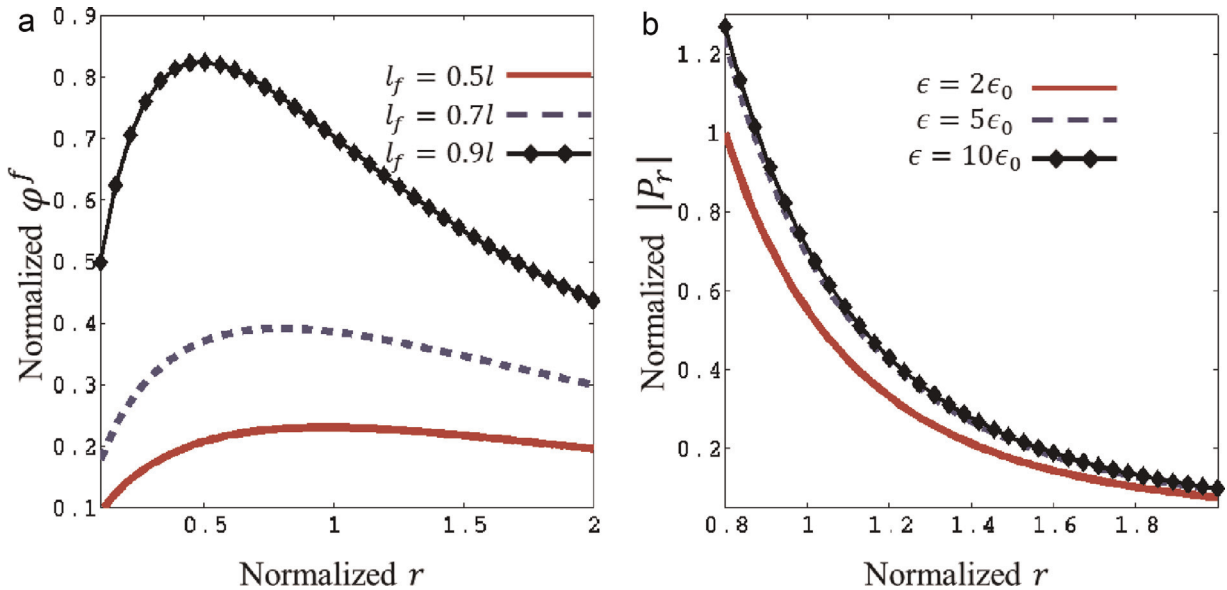


Fig. 2. (a) plots radial distribution of electric potential at $\theta = \pi/2$, with various l_f 's. The electric potential is significant only close to the dislocation. A large l_f accentuates the peaks in the curves. (b) plots the radial polarization field with different dielectric constants. We clearly observe that the curves almost overlap when dielectric constant is larger than 5. All quantities here are normalized, with potential ϕ^f by ϕ^m , polarization $|P_r|$ normalized by $|P^m|$ and radial coordinates r by the SGE length scale l .

$$\theta^0 = -\frac{b_x \sin \theta}{2\pi\sigma r}, \quad \Omega^0 = -\frac{b_x \cos \theta}{2\pi r}. \quad (34)$$

Following the methods used in Lazar and Maugin (2006) we obtain

$$\theta = -\frac{b_x \sin \theta}{2\pi\sigma r} [1 - \gamma K_1(\gamma)], \quad \Omega = -\frac{b_x \cos \theta}{2\pi r} [1 - \gamma_2 K_1(\gamma_2)], \quad (35)$$

where γ is defined as r/l_0 , as for the point defect, $\gamma_2 = r/l_2$ and $K_1(x)$ is a modified Bessel function of the second kind. It can be shown that the above results converge to classical linear elasticity when $l \rightarrow 0$, $f_1, f_2 \rightarrow 0$ and to SGE when $f_1, f_2 \rightarrow 0$. A direct consequence of the above solution is the associated electric potential:

$$\varphi^f = \frac{fb_x \sin \theta}{2\pi a \epsilon \sigma r} [1 - \gamma K_1(\gamma)] = \varphi^{fm} \left[\frac{1}{\gamma} - K_1(\gamma) \right] \sin \theta, \quad (36)$$

where $\varphi^{fm} = fb_x / (2\pi a \epsilon \sigma l_0)$. This potential is only related to the bulk flexoelectric length scale l_0 . It reaches its maximum around l_0 , as plotted in Fig. 2(a), and decays to 0 in the both limits of $\gamma \gg 1$ and $\gamma \ll 1$:

$$\varphi^f \sim \frac{1}{\gamma} \text{ when } \gamma \gg 1; \quad \varphi^f \sim -\gamma \ln 2\gamma \text{ when } \gamma \ll 1. \quad (37)$$

Generally speaking, in single crystals the length scale l_0 and l are comparable to b_x (Maranganti and Sharma, 2007). Therefore, strain-gradient induced electric potential is significant only in the vicinity of the core, namely when $r \sim l$. Moreover, the electric field, as the negative gradient of this potential, has the appearance of a Lennard-Jones potential – the field decays strongly when $r < l_0$, reaches a minimum, and then increases slowly for $r > l_0$. The magnitude of the electric field dies down in the far field, but reaches a maximum in the vicinity of $r \sim 2l_0$, still in the range $r \sim l$. In that region:

$$\varphi^{fm} \sim 1\text{--}10 \text{ V}, \quad |\mathbf{E}|^m \approx 1 \times 10^7\text{--}1 \times 10^8 \text{ V/cm}, \quad (38)$$

since $l_0 \approx 10^{-9} \text{ m}$ (Nowacki, 2006) and $f \sim 1\text{--}10 \text{ V}$ (Zubko et al., 2013) (this is a conservative estimate of f). Interestingly, Turchányi et al. (1973) reported from their experiments decades ago, that in alkali halide crystals, the field generated by a “charged” dislocation is in the range of $3.5 \times 10^6\text{--}1.05 \times 10^7 \text{ V/cm}$. This is in good agreement with our estimates above.

These dislocations are called “charged” because they create non-zero electric field and electric potential. This does not violate Eq. (1) since the “free charge” density ρ^e is still zero. Since the total charge is the sum of free charge and polarized (or bound) charge, it is possible that the dislocation generates non-vanishing electric field without carrying any free charge. Here the polarized charge arises due to the flexoelectric effect.

We can also compute the polarization field around the dislocation using the isotropic constitutive equations (Mao and Purohit, 2014):

$$P_i = -a^{-1}[\varphi_i + f_1 u_{k,ki} + f_2 (u_{j,ji} + u_{i,jj})] = -a^{-1}(\varphi_i + f\theta_{,i} + f_2 e_{i3j}\Omega_j). \quad (39)$$

In polar coordinates the polarization field is

$$P_r = -\frac{P^m \sin \theta}{(r/l)^2} \left\{ \frac{\epsilon_0}{\epsilon\sigma} \left[1 + \gamma K_1(\gamma) + \gamma^2 K_0(\gamma) \right] - \frac{f_2}{f} \left[1 + \gamma_2 K_1(\gamma_2) \right] \right\}, \quad (40)$$

$$P_\theta = \frac{P^m \cos \theta}{(r/l)^2} \left\{ \frac{\epsilon_0}{\epsilon\sigma} \left[1 + \gamma K_1(\gamma) \right] - \frac{f_2}{f} \left[1 + \gamma_2 K_1(\gamma_2) + \gamma_2^2 K_0(\gamma_2) \right] \right\}, \quad (41)$$

where $P^m = b_x f / (2\pi a l^2)$. Unlike the potential we have both γ and γ_2 present in these equations. However, in most cases, the polarization will be dominated by the γ_2 , and hence f_2 terms. This is evident from Fig. 2(b) in which we see that curves for dielectric constant of 5 and 10 are almost identical. For most solids in which flexoelectricity is prominent, dielectric constant is 10^2 or more. In perovskite materials, for which it is more than 10^3 , we can safely claim that the polarization field around an edge dislocation is determined by f_2 .

From the polarization field, we are able to estimate the line charge density of the dislocation and compare it with the experiments done by Petrenko and Whitworth (1983) on charged dislocations in ice. Again, as indicated above, the “charge” that we are referring to is the charge due to polarization rather than the free charge. The polarized line charge density λ^e can be written as

$$\lambda^e \approx Pl_0 \approx \frac{1.6\epsilon b_x f_2}{\pi l_0}. \quad (42)$$

Since the dielectric constant of ice is around 100 (Hobbs et al., 1966) the polarization must be dominated by the f_2 term. From the data given in Petrenko and Whitworth (1983), we know $l_0 \approx 50 \mu\text{m}$, $b_x \approx 0.73a \sim 10^{-9} \text{ m}$, and from Zubko et al. (2013) $f \sim 1\text{--}10 \text{ V}$, hence

$$\lambda^e \approx 0.01\text{--}0.1 \text{ pC/m} \sim 10^{-4}\text{--}10^{-3}e/a, \quad (43)$$

where a is the lattice parameter and e is the electron charge. The line charge density measured in the experiments is $\lambda^e = 3.0 \times 10^{-3}e/a$, reasonably close to our rough estimate. This suggests that flexoelectricity could provide a plausible reason for charged dislocations in ice.

Besides ice, perovskite materials like barium titanate and strontium titanate (STO) are good candidates to observe interplay between dislocations and flexoelectricity. These materials have larger flexoelectric and dielectric constants and much shorter screening length scale l_0 (especially, in single crystals) (Maranganti and Sharma, 2007). For example, Zubko et al. (2007) measured the polarization constant of STO to be around 1–10 nC/m. This suggests that the charges around a dislocation would be on the order of $10^4\text{--}10^5 \mu\text{C/m}^2$ at room temperature in STO. At lower temperatures the dielectric constant is even higher, so there will be more charge near the dislocation. This is a prediction from our analysis that could be verified against experiments.

5. Crack mechanics

We now extend our analysis to cracks in flexoelectric solids. Since crack tip fields are singular there are large gradients near the tips. Thus, we expect flexoelectricity to play a prominent role in determining the intensity factors. To tease out the contribution of flexoelectricity we will perform an asymptotic analysis of crack tip fields in flexoelectric solids. We expect that the effects of flexoelectricity will die out far enough away from the crack tips just as we observed for point defects and dislocations. Here we follow the notation as in Mao and Purohit (2014), where T_{ij} is the stress and \hat{T}_{ijk} is the higher-order stress.

5.1. Mode III crack

We start by considering a semi-infinite Mode III crack along the x_1 -axis with crack tip located at the origin. This is an anti-plane shear problem with out-of-plane displacement $u_3 = w$ and an electric potential φ . They are homogeneous along the x_3 -axis but functions of in-plane coordinates, x_1 and x_2 . The only surviving stresses are shear stresses T_{i3} and T_{3i} with $i=1,2$. Recall that the antiplane shear version of the governing equation is (Mao and Purohit, 2014)

$$\nabla^2 \varphi = 0, \quad (1 - l_2^2 \nabla^2) \nabla^2 w = 0. \quad (44)$$

As for the boundary conditions, we require that the crack faces are traction free, so that at $\theta = \pm \pi$:

$$t_3 = T_{23} - \hat{T}_{123,1} - \hat{T}_{223,2} - \hat{T}_{213,1} = 0, \quad (45)$$

$$r_3 = \hat{T}_{223} = 0. \quad (46)$$

We have used a cylindrical coordinates here with $x_1 = r \cos \theta$ and $x_2 = r \sin \theta$. We also impose the impermeable electric boundary condition:

$$D_2 = 0 \quad \text{at } x_2 = 0, x_1 < 0. \quad (47)$$

For example, this is a good approximation for cracks in ceramics with air between the open crack faces. We also require that far away from the crack tip the electric field and electric displacement decay to zero. The above imply that the in-plane component of \mathbf{E} and \mathbf{D} admit only the trivial solution, thus being irrelevant for our problem. From the constitutive equations we have

$$T_{i3} = \mu w_{,i}, \quad \hat{T}_{i13} = \mu l^2 [w_{,ii} - \alpha^2 \nabla^2 w], \quad (48)$$

$$\hat{T}_{123} = \hat{T}_{213} = \mu l^2 w_{,12}, \quad P_3 = -(\epsilon - \epsilon_0) f_2 \nabla^2 w \quad (49)$$

where $\alpha^2 = f_2^2 / \mu a l^2$. We require $\alpha^2 \leq 1/2$ (see the Appendix).

To find the asymptotic crack tip solution we assume that $w = r^s F_s(\theta)$. Then the leading order solution is

$$w(r, \theta) = C_3 \sqrt{\frac{r^3}{l}} \left[\sin \frac{\theta}{2} - \left(\frac{5}{3} - \frac{8}{3} \alpha^2 \right) \sin \frac{3\theta}{2} \right], \quad (50)$$

with C_3 being an undetermined constant which generally depends on l . In fact, C_3 is related to the stress intensity factor. Note in the above asymptotic solution that as l and α tend to 0, $w(r, \theta)$ tends to the classical solution from linear elastic fracture mechanics. This idea will come up again when we compute the energy release rate. When we let $\alpha \rightarrow 0$, the solution converges to the SGE version of the crack problem, with just the pre-factor to be determined (Zhang et al., 1998).

An interesting result emerging from this displacement field is that an out-of-plane polarization is expected:

$$P_3 = \frac{f_2 C_3}{2a\sqrt{rl}} \sin \frac{\theta}{2}, \quad \lim_{r \rightarrow 0} \sqrt{\frac{r}{l}} P_3(r, \frac{\pi}{2}) = \frac{\sqrt{2} f_2 C_3}{4al}. \quad (51)$$

This polarization is independent of z . This prediction could perhaps be verified in an experiment.

5.2. Planar cracks

The solution of the asymptotic crack tip fields in Mode III involves solving a simpler problem than Mode I and Mode II. But, in the Mode III solution we saw some essential features of the crack-tip fields that will be present also for Mode I and Mode II cracks. The key difference between plane cracks of Mode I and II as opposed to Mode III is that the dilatation gradient (which is directly proportional to the hydro-static pressure gradient) induces a non-trivial electric field around plane cracks. This fact was utilized by Petrenko to explain how “pseudo-piezoelectricity” could lead to emission of electromagnetic radiation from a steadily moving crack in glacial ice (Petrenko, 1996).

For simplicity, we will discuss only the plane strain version of this problem. Here we have, $u_i = u_i(x_1, x_2)$, $i = 1, 2$ and $u_3 = 0$. Recall the governing equations (1) and (2). Let $\theta = u_{k,k}$ be the dilatation. Taking the divergence on both sides of (2) the governing equations become

$$\nabla^2(a\epsilon\varphi + f\theta) = 0, \quad (52)$$

$$(1 - l_0^2 \nabla^2) \nabla^2 \theta = 0. \quad (53)$$

In order to find the crack tip asymptotic solution, we will again assume $u_i = r^s F_s^{(i)}(\theta)$ and $\varphi = r^s G_s(\theta)$. Then, the solutions that have a $r^{1/2}$ singularity are

$$\theta = r^{1/2} (c_1 \cos \frac{\theta}{2} + c_2 \cos \frac{3\theta}{2} + c_3 \sin \frac{\theta}{2} + c_4 \sin \frac{3\theta}{2}), \quad (54)$$

$$\varphi = r^{1/2} (c_5 \cos \frac{\theta}{2} + c_6 \sin \frac{\theta}{2}) - \frac{f}{a\epsilon} \theta, \quad (55)$$

where c_i , $i=1-6$, are all constants to be determined. We will now discuss the (displacement) symmetric mode (Mode I) and anti-symmetric mode (Mode II) separately, in both pure insulating and pure conducting case. We will also discuss the mixture of (electrical and mechanical) modes. Since (52) contains only partial information of the governing equation, we will need another equation to complete the solution. We will follow the approach of Aravas and Giannakopoulos (2009).

5.2.1. Mode I, pure insulating/conducting

For a Mode I crack we require that $u_r(r, \theta) = u_r(r, -\theta)$ and $u_\theta(r, \theta) = -u_\theta(r, -\theta)$. Without loss of generality, we can assume the following:

$$u_r = \sqrt{\frac{r^3}{l}} (A_1 + A_2 \cos \theta + A_0 \cos 2\theta) \cos \frac{\theta}{2}, \quad (56)$$

$$u_\theta = \sqrt{\frac{r^3}{l}} (A_3 + A_4 \cos \theta - A_0 \cos 2\theta) \sin \frac{\theta}{2}, \quad (57)$$

$$\theta = \sqrt{\frac{r}{16l}} \left[(10A_1 + 5A_2 + 2A_3 - A_4) \cos \frac{\theta}{2} + (3A_4 + 5A_2 + 8A_0) \cos \frac{3\theta}{2} \right], \quad (58)$$

$$\varphi = -\frac{f}{a\epsilon} \left[\sqrt{\frac{r}{l}} \left(A_5 \cos \frac{\theta}{2} + A_6 \sin \frac{\theta}{2} \right) + \theta \right], \quad (59)$$

where A_i 's are all unknown constants. Our goal is to determine these constants by insisting that the governing equations and boundary conditions are satisfied. The above electric potential is of the general asymptotic form that satisfies (1).

By differentiating the electric potential we see that the electric field components are

$$E_r = \frac{f}{8ael} \sqrt{\frac{l}{r}} \left[(10A_1 + 5A_2 + 2A_3 - A_4 + 4A_5) \cos \frac{\theta}{2} + (3A_4 + 5A_2 + 8A_0) \cos \frac{3\theta}{2} + 4A_6 \sin \frac{\theta}{2} \right], \quad (60)$$

$$E_\theta = -\frac{f}{8ael} \sqrt{\frac{l}{r}} \left[(10A_1 + 5A_2 + 2A_3 - A_4 + 4A_5) \sin \frac{\theta}{2} + 3(3A_4 + 5A_2 + 8A_0) \sin \frac{3\theta}{2} - 4A_6 \cos \frac{\theta}{2} \right]. \quad (61)$$

Then, by constitutive laws (Mao and Purohit, 2014), we compute the polarization:

$$P_r = \frac{1}{a} [E_r - f_2 \left(\nabla^2 u_r - \frac{u_r}{r^2} - \frac{2}{r^2} \frac{\partial u_\theta}{\partial \theta} \right) - (f_1 + f_2) \frac{\partial \Theta}{\partial r}], \quad (62)$$

$$P_\theta = \frac{1}{a} [E_\theta - f_2 \left(\nabla^2 u_\theta - \frac{u_\theta}{r^2} + \frac{2}{r^2} \frac{\partial u_r}{\partial \theta} \right) - (f_1 + f_2) \frac{\partial \Theta}{r \partial \theta}]. \quad (63)$$

By the constitutive equation $D_i = \epsilon_0 E_i + P_i$, we can determine the electric displacement easily and show that this D_i is indeed divergence-free. We now turn to the mechanics part of this problem. The strains are

$$S_{rr} = \frac{3}{2} \sqrt{\frac{r}{l}} (A_1 + A_2 \cos \theta + A_0 \cos 2\theta) \cos \frac{\theta}{2}, \quad (64)$$

$$S_{\theta\theta} = -\frac{1}{2} \sqrt{\frac{r}{l}} [2A_4 - 2A_1 + 4A - A_3 - (8A_0 + 3A_4 + 2A_2) \cos \theta + 3A_0 \cos 2\theta] \cos \frac{\theta}{2}, \quad (65)$$

$$S_{r\theta} = -\frac{1}{4} \sqrt{\frac{r}{l}} [2A_2 - A_3 + 4A_0 + A_1 + (3A_2 + 8A_0 - A_3) \cos \theta + 6A_0 \cos 2\theta] \sin \frac{\theta}{2}. \quad (66)$$

From the constitutive law (Mao and Purohit, 2014) the stresses are

$$T_{rr} = (\lambda + 2\mu)S_{rr} + \lambda S_{\theta\theta}, \quad T_{\theta\theta} = (\lambda + 2\mu)S_{\theta\theta} + \lambda S_{rr}, \quad T_{r\theta} = T_{\theta r} = 2\mu S_{r\theta}. \quad (67)$$

The higher order stresses are given by

$$\begin{aligned} \hat{T}_{rrr} &= l^2 T_{rr,r} + f P_r, & \hat{T}_{r\theta\theta} &= l^2 T_{\theta\theta,r} + f_1 P_r, & \hat{T}_{rr\theta} &= \hat{T}_{r\theta r} = l^2 T_{r\theta,r} + f_2 P_\theta, \\ \hat{T}_{\theta rr} &= l^2 r^{-1} (T_{rr,\theta} - 2T_{r\theta}) + f_1 P_\theta, & \hat{T}_{\theta\theta\theta} &= l^2 r^{-1} (T_{\theta\theta,\theta} + 2T_{r\theta}) + f P_\theta, \\ \hat{T}_{\theta r\theta} &= \hat{T}_{\theta\theta r} = l^2 r^{-1} (T_{r\theta,\theta} + T_{rr} - T_{\theta\theta}) + f_2 P_r. \end{aligned} \quad (68)$$

For convenience we also compute $p_{jk} = \hat{T}_{ijk,i}$:

$$p_{rr} = \frac{\partial \hat{T}_{rrr}}{\partial r} + \frac{1}{r} \frac{\partial \hat{T}_{\theta rr}}{\partial \theta} + \frac{\hat{T}_{rrr} - 2\hat{T}_{\theta r\theta}}{r}, \quad (69)$$

$$p_{r\theta} = \frac{\partial \hat{T}_{rr\theta}}{\partial r} + \frac{1}{r} \frac{\partial \hat{T}_{\theta r\theta}}{\partial \theta} + \frac{\hat{T}_{rr\theta} + \hat{T}_{\theta rr} - \hat{T}_{\theta\theta\theta}}{r}, \quad (70)$$

$$p_{\theta\theta} = \frac{\partial \hat{T}_{r\theta\theta}}{\partial r} + \frac{1}{r} \frac{\partial \hat{T}_{\theta\theta\theta}}{\partial \theta} + \frac{\hat{T}_{r\theta\theta} + 2\hat{T}_{\theta r\theta}}{r}. \quad (71)$$

Now we are ready to plug these into the governing equations. The equilibrium equation is given by (Mao and Purohit, 2014)

$$T_{jk,j} - \hat{T}_{ijk,ij} = 0. \quad (72)$$

We substitute for T_{jk} and \hat{T}_{ijk} , then to leading order this boils down to

$$p_{rr,\theta} + r^{-1} (p_{r\theta,\theta} + p_{rr} - p_{\theta\theta}) = 0. \quad (73)$$

Note that this is just one of the two equilibrium equations. However, this equation and (52) are the full governing equations for the flexoelectric crack problem. As in LEFM, here we assume traction free boundary conditions along the faces of our semi-infinite crack. So, the traction and higher order traction are both zero on the crack faces (Aravas and Giannakopoulos, 2009). We have not put any restrictions on electric part of the solution other than the governing equation it has to satisfy. From the traction free conditions, we find that at $\theta = \pm \pi$:

$$t_{r\theta} = -p_{r\theta} - \hat{T}_{\theta rr,r} = 0, \quad (74)$$

$$t_{\theta\theta} = -p_{\theta\theta} - \hat{T}_{\theta r\theta,r} = 0, \quad (75)$$

$$\hat{T}_{\theta\theta r} = \hat{T}_{\theta\theta\theta} = 0. \quad (76)$$

The second and third of these boundary conditions boil down to

$$t_{\theta\theta} = -\frac{\alpha\beta\mu A_6}{4} \left(\frac{r}{l} \right)^{-3/2} = 0, \quad (77)$$

$$\hat{I}_{\theta\theta r} = \frac{\alpha\beta\mu l A_6}{2} \left(\frac{r}{l}\right)^{-1/2} = 0. \quad (78)$$

Hence, if we insist on the traction-free boundary condition then A_6 must vanish.

Before starting the discussion on the electric part of the solution, we introduce some non-dimensional material constants $\alpha = f_2/(l\sqrt{a\mu})$, $\beta = f/(l\sqrt{a\mu})$ and ν the Poisson ratio. We will also use the relation $a\epsilon \approx 1$, which is typical for solids with large dielectric constants and are the main focus of this study. Following Aravas and Giannakopoulos (2009), we define intensity constants, C_{11} and C_{12} , which are given by

$$G_{11} = -\lim_{r \rightarrow 0} \frac{u_\theta(r, \pi)}{\sqrt{r^3/l}}, \quad G_{12} = -\lim_{r \rightarrow 0} \frac{\Omega(r, \pi)}{\sqrt{r/l}}. \quad (79)$$

Here, Ω as defined in (27) is the rotation of the displacement field.

Now, we turn to the electric part of the solution. First, let us consider the Mode I pure impermeable/insulating crack boundary condition:

$$D_\theta(r, \pm \pi) = 0, \quad D_\theta(r, 0) = 0. \quad (80)$$

By imposing this boundary condition (since $A_6 = 0$, $D_\theta(r, 0) = 0$ is already satisfied), the solution to D_θ is

$$\frac{D_\theta}{\sqrt{\mu\epsilon}} = \frac{\alpha(3C_{11} - 2C_{12})}{8(1 - \alpha^2)} \left(\sin \frac{\theta}{2} + \sin \frac{3\theta}{2} \right) \sqrt{\frac{l}{r}}. \quad (81)$$

Since the D_θ component of electric displacement is 0 behind and ahead of the crack tip it does not contribute to the J integral (as will become clear later). Even though D_θ vanishes, the corresponding electric field component at $\theta = \pm \pi$ does not:

$$\frac{E_\theta(r, \pi)}{\sqrt{\mu/\epsilon}} = \frac{(3C_{11} - 4C_{12})(2\nu - 1)\beta + 4C_{12}(1 - \nu)\alpha}{4(1 - \nu)} \sqrt{\frac{l}{r}}. \quad (82)$$

For the Mode I pure conducting case, the boundary conditions are

$$E_r(r, 0) = 0, \quad E_r(r, \pm \pi) = 0. \quad (83)$$

Again, this makes that the contribution of the electric part to the J integral vanishes. The solution is

$$\frac{E_r(r, \theta)}{\sqrt{\mu/\epsilon}} = \frac{(3C_{11} - 2C_{12})\beta}{16\sigma} \left(\cos \frac{\theta}{2} - \cos \frac{3\theta}{2} \right) \sqrt{\frac{l}{r}}, \quad (84)$$

where $\sigma = (1 - \nu)/(1 - 2\nu)$ is a material constant which we used for the edge dislocation. Along the crack faces, $E_\theta(r, \pi)$ is given by

$$\frac{E_\theta(r, \pi)}{\sqrt{\mu/\epsilon}} = \frac{\beta(3C_{11} - 4C_{12})}{4\sigma} \sqrt{\frac{l}{r}}. \quad (85)$$

The fact that the electric field perpendicular to the crack face does not vanish and is proportional to $1/\sqrt{r}$ asymptotically is of interest. Imagine a steadily growing crack so that, $r = r(t)$ and E_θ is a function of time t as well. If the crack is moving quasistatically along the x_1 -axis at a constant speed ν , then we know $\dot{E}_\theta \propto r^{-3/2}\nu$. According to the Maxwell equations, this will induce a magnetic field. Hence a growing crack in a flexoelectric solid will emit radiation. This was observed in a series of experiments by Petrenko and co-workers for cracks in ice (Petrenko, 1996). The simple model they used postulated that the electric field is proportional to the hydro-static pressure gradient. In our analysis it is the flexoelectric constant f that relates them. Hence, the experiments carried out by Petrenko and co-workers strongly support their idea that “pseudo-piezoelectricity” (or flexoelectricity) is responsible for radiation emitted from sliding glaciers.

However, unlike Petrenko and co-workers (Petrenko, 1996) who simply use the results from LEFM to deduce the potential field, here we have provided a solution that satisfies both the mechanical and electrical governing equations. We see that the field produced around the crack tip is indeed asymptotically similar to that in the piezoelectric case, both $r^{-1/2}$. However, ice is not piezoelectric, so the flexoelectric effect could very likely be the cause behind the effects seen by Petrenko and co-workers. Aside from the postulates about the coupling between the gradients of hydrostatic pressure/dilatation and polarization, there are also couplings that come from the gradients of shear stresses/strains which are also prominent around the crack tip and included in our analysis.

5.2.2. Mode II, pure insulating/conducting

For a Mode II crack we require that $u_r(r, \theta) = -u_r(r, -\theta)$ and $u_\theta(r, \theta) = u_\theta(r, -\theta)$. Without loss of generality, we can assume the following:

$$u_r = \sqrt{\frac{r^3}{l}} (B_1 + B_2 \cos \theta + B_0 \cos 2\theta) \sin \frac{\theta}{2}, \quad (86)$$

$$u_\theta = \sqrt{\frac{r^3}{l}} (B_3 + B_4 \cos \theta + B_0 \cos 2\theta) \cos \frac{\theta}{2}, \quad (87)$$

$$\theta = \sqrt{\frac{r}{16l}} \left[(10B_1 + 5B_2 + 2B_3 - B_4) \sin \frac{\theta}{2} + (3B_4 + 5B_2 + 8B_0) \sin \frac{3\theta}{2} \right], \quad (88)$$

$$\varphi = -\frac{f}{a\epsilon} \left[\sqrt{\frac{r}{l}} \left(B_5 \sin \frac{\theta}{2} + B_6 \cos \frac{\theta}{2} \right) + \theta \right], \quad (89)$$

where B_i 's are all unknown constants. In order to find all B_i 's we carry out the same calculations as in the Mode I case. The crack faces $\theta = \pm \pi$ are again assumed to be free of tractions and higher order tractions. At $\theta = 0$ we assume that all the fields are continuous. Again, due to the traction free boundary conditions:

$$t_{\theta r} = -\frac{\beta^2 \mu B_6}{4} \left(\frac{r}{l} \right)^{-3/2} = 0, \quad (90)$$

$$\hat{I}_{\theta\theta\theta} = \frac{\beta^2 \mu l B_6}{2} \left(\frac{r}{l} \right)^{-1/2} = 0, \quad (91)$$

so that $B_6 = 0$. For the same reason as in Mode I, the displacement field can be fully determined by the following intensity constants to C_{21} and C_{22} :

$$C_{21} = \lim_{r \rightarrow 0} \frac{S_{\theta r}(r, \theta = 0)}{\sqrt{r/l}}, \quad C_{22} = -\lim_{r \rightarrow 0} \frac{\Omega(r, \theta = 0)}{\sqrt{r/l}}. \quad (92)$$

Now, consider the pure insulating and pure conducting crack boundary conditions just as we did in Mode I. For the pure insulating case, we have the following solution for D_θ :

$$\frac{D_\theta(r, \theta)}{\sqrt{\mu\epsilon}} = -\frac{\alpha C_{21}}{1 + \alpha^2(2\nu - 3)} \left(\cos \frac{\theta}{2} - \cos \frac{3\theta}{2} \right) \sqrt{\frac{l}{r}}. \quad (93)$$

For the pure conducting case, we have

$$\frac{E_r(r, \theta)}{\sqrt{\mu|\epsilon}} = \frac{\alpha C_{21}(1 - \alpha^2)\beta(2\nu - 1)}{2 + 2\alpha^2(2\nu - 3)} \left(\sin \frac{\theta}{2} + \sin \frac{3\theta}{2} \right) \sqrt{\frac{l}{r}}. \quad (94)$$

Again, for both purely insulating and conducting cases the electric contribution to the J integral is zero.

5.2.3. Mode D and Mode E

Just as in Mode I and Mode II cracks, the displacement fields for Mode D (insulating, zero traction) and Mode E (conducting, zero traction) are determined by C_{ij} , $i, j = 1, 2$. Generally, when a crack is conducting, we define the electric field intensity factor K_E as

$$K_E = \lim_{r \rightarrow 0} \sqrt{2\pi r} E_r(r, 0). \quad (95)$$

For insulating cracks we define K_D as

$$K_D = \lim_{r \rightarrow 0} \sqrt{2\pi r} D_\theta(r, 0). \quad (96)$$

The boundary conditions for Mode D are

$$t_{\theta\theta} = t_{\theta r} = 0, \quad D_\theta = \frac{K_D}{\sqrt{2\pi r}} \text{ at } \theta = 0. \quad (97)$$

This is the case in which the relevant stresses and higher-order stresses are zero along crack line, therefore The sole contribution to the J integral comes from the electrical part. In order to find C_{ij} we have to impose two more conditions on the higher order tractions since we have a gradient theory:

$$\hat{I}_{\theta\theta r} = \hat{I}_{\theta\theta\theta} = 0 \quad \text{at } \theta = 0. \quad (98)$$

All these lead to

$$G_{11} = C_{12} = C_{21} = 0, \quad (99)$$

$$C_{22} = \frac{K_D}{\sqrt{2\pi\mu\ell}} [2\alpha(1-\nu) - \beta(1-2\nu)]. \quad (100)$$

The boundary conditions for Mode E are, at $\theta = 0$:

$$t_{\theta\theta} = t_{\theta r} = 0, \quad E_r = \frac{K_E}{\sqrt{2\pi r}}, \quad (101)$$

$$\hat{T}_{\theta\theta r} = \hat{T}_{\theta\theta\theta} = 0. \quad (102)$$

On the crack faces, $\theta = \pm\pi$, traction and higher-order traction are zero and $E_r = 0$. These conditions give

$$C_{21} = C_{22} = 0, \quad (103)$$

$$G_{11} = \frac{(K_E/3)}{\sqrt{2\pi\mu\ell/\epsilon}} \left[\frac{2\alpha(1-\nu) - \beta(1-2\nu)}{1 - \alpha^2 - (1-2\nu)(\beta - \alpha)^2} \right], \quad (104)$$

$$G_{12} = \frac{(K_E/2)}{\sqrt{2\pi\mu\ell/\epsilon}} \left[\frac{2\alpha(1-\nu) - \beta(1-2\nu)}{1 - \alpha^2 - (1-2\nu)(\beta - \alpha)^2} \right]. \quad (105)$$

5.2.4. Mixed modes

The classification above separates mechanical and electrical boundary loads. In practice, when we are dealing with cracks in electromechanically active materials, it is difficult to completely separate mechanical modes and electrical modes. As mentioned in a recent review of closely related piezoelectric fracture (Kuna, 2010), “mechanical and electrical quantities are inherently coupled at the crack” and “there is always a mixture of (mechanical and electrical) crack opening modes”. For this reason we give some results on mixed modes below.

Recall the boundary conditions of the pure conducting case which result in $K_E=0$, and the pure insulating case which result in $K_D=0$. Now, let us imagine a crack under Mode I loading. From the fact that $A_6 = 0$ (traction-free faces), we know that $D_\theta(r, 0) = 0$ before we impose any electric boundary condition (as discussed in Mode I pure insulating crack). Also, recall that in Mode D all constants related to Mode I, i.e. G_{11}, G_{12} are zero. This means that in a flexoelectric solid, Mode I cannot be mixed with Mode D (under the traction free faces assumption). If we forcefully introduce Mode D together with Mode I, then C_{22} will be non-zero, and the crack will have a Mode II component too. A similar argument shows that Mode II cannot be mixed with Mode E under the current framework.

On the other hand, since the Mode I solution does not exclude the possibility of non-zero K_E , we can have a crack in which Mode I pure conducting conditions are mixed with Mode E. Then, the boundary condition is different from that of the Mode I pure conducting case, viz.,

$$E_r(r, \pm\pi) = 0, \quad E_r(r, 0) = \frac{K_E}{\sqrt{2\pi r}}. \quad (106)$$

We have computed the strain profiles for this boundary condition. For the purposes of illustration we picked a particular set of material parameters: $\alpha = 0.5$, $\beta = 0.6$, $\nu = 0.3$. Then, the strain profile is

$$S_{rr} = \left[(0.009G_{11} - 0.11G_{12} + 0.21K_4^I) \cos \frac{\theta}{2} + (-0.76G_{11} + 0.51G_{12}) \cos \frac{3\theta}{2} \right. \\ \left. + \left(1.04G_{11} - 0.87G_{12} - 0.043K_4^I \right) \cos \frac{5\theta}{2} \right] \sqrt{\frac{r}{l}}, \quad (107)$$

$$S_{r\theta} = \left[(-0.043G_{11} + 0.098G_{12} - 0.24K_4^I) \sin \frac{\theta}{2} + (0.56G_{11} - 0.37G_{12}) \sin \frac{3\theta}{2} \right. \\ \left. + \left(0.87G_{11} - 0.043G_{12} - 1.04K_4^I \right) \sin \frac{5\theta}{2} \right] \sqrt{\frac{r}{l}}, \quad (108)$$

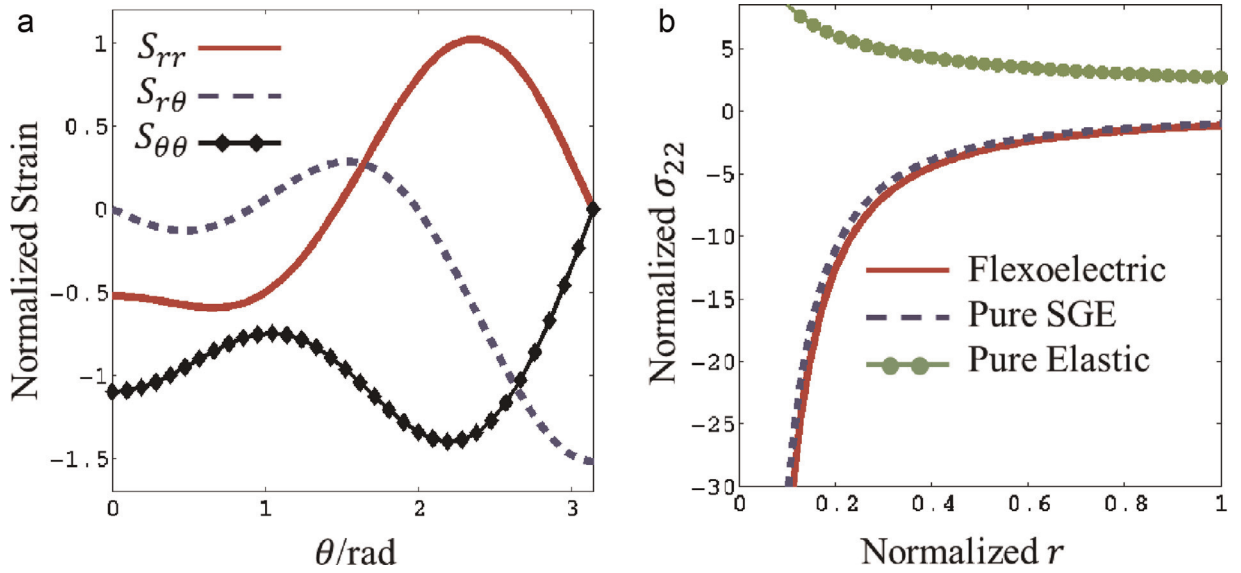


Fig. 3. (a) plots the strain profiles at $r=l$ as a function of θ for a Mode I crack. (b) plots the normalized σ_{22} at $\theta = \pi/2$ for a Mode I crack in an isotropic linear elastic solid, a linear SGE solid and a flexoelectric solid. We used material constants $\alpha = 0.5$, $\beta = 0.6$, $\nu = 0.3$. The intensity factors we used for (a) and the flexoelectric curve in (b) are $G_1 = 3.30$, $G_2 = 3.433$, $K_4^I = 1.0$. For SGE in (b), they are $G_1 = 3.061$, $G_2 = 3.433$, chosen according to Tsantidis and Aravas (2011). The flexoelectric intensity factors and elastic intensity factors are chosen such that the energy release rate is fixed. Details of the energy release rate can be found in a later section. σ_{22} are normalized against μ , the shear modulus, and r against the SGE length scale l , as in other graphs.

$$S_{\theta\theta} = \left[(0.21G_1 - 0.60G_2 + 0.13K_4^I) \cos \frac{\theta}{2} + (0.55G_1 - 0.37G_2) \cos \frac{3\theta}{2} \right. \\ \left. + [-1.04G_1 + 0.87G_2 + 0.043K_4^I] \cos \frac{5\theta}{2} \right] \sqrt{\frac{r}{l}}. \quad (109)$$

These are plotted in Fig. 3(a) for $r=l$. Notice that instead of using K_E we introduce, for convenience, a non-dimensional constant K_4^I , which is a linear combination of C_{11} , C_{12} and K_E (detailed expression in Appendix). It is defined as

$$K_4^I = \lim_{r \rightarrow 0} \sqrt{\frac{r}{\mu \epsilon l}} D_\theta(r, \pi). \quad (110)$$

We also compute true stress σ_{22} (as defined in Aravas, 2011) for the above-mentioned material parameters, as depicted in Fig. 3(b). The similarity between the SGE solution and the flexoelectric solution is clear. Interestingly enough, the σ_{22} plot suggests compression just behind the crack tip, a feature also observed by Aravas and Giannakopoulos (2009).

For the same material parameters the strain profile for a Mode II pure insulating crack mixed with Mode D is

$$S_{rr} = \left[(-0.03C_{21} + C_{22} - 0.63K_4^{II}) \sin \frac{\theta}{2} - 2.67 \sin \frac{3\theta}{2} + (2.61C_{21} + 0.125K_4^{II}) \sin \frac{5\theta}{2} \right] \sqrt{\frac{r}{l}}, \quad (111)$$

$$S_{r\theta} = \left[(-0.34C_{21} - 0.13K_4^{II}) \cos \frac{\theta}{2} - 1.95C_{21} \cos \frac{3\theta}{2} + (2.61C_{21} - 0.13K_4^I) \cos \frac{5\theta}{2} \right] \sqrt{\frac{r}{l}}, \quad (112)$$

$$S_{\theta\theta} = \left[(-0.72C_{21} + C_{22} - 0.38K_4^{II}) \sin \frac{\theta}{2} + 1.92 \sin \frac{3\theta}{2} - (2.61C_{21} + 0.13K_4^I) \sin \frac{5\theta}{2} \right] \sqrt{\frac{r}{l}}. \quad (113)$$

Here again, for convenience, a non-dimensionalized intensity K_4^{II} is used instead of K_D :

$$K_4^{II} = K_D / \sqrt{2\pi\mu\epsilon l}. \quad (114)$$

As discussed in the beginning of this section, Mode II cannot be mixed with Mode E.

Notice that we have not used the conventional intensity factors K_I , K_{II} etc., because their expressions are lengthy and cumbersome. However, those conventional intensity factors can be written in terms of C_{11} , C_{12} , K_4^I and C_{21} , C_{22} , K_4^{II} as shown in the Appendix. Using the constants defined above we can work out the displacement, strain and stress profiles. The expressions are long and are not reproduced here.

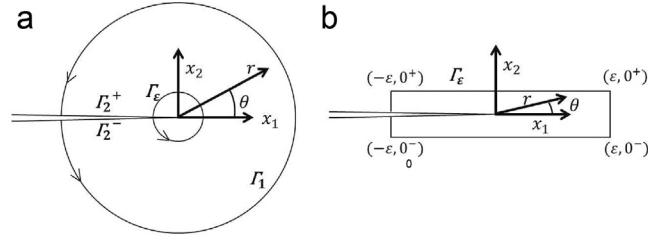


Fig. 4. Contours used in computation of the energy release rate. We use the circular contour for the Mode III crack and the box contour for Mode I and Mode II cracks. (a) Circular contour. (b) Box contour.

5.3. J integral

In analogy to piezoelectricity, the flexoelectric energy momentum tensor can be written as

$$Q_{ik} = H\delta_{ik} - \sigma_{ij}u_{j,k} - \hat{T}_{ijl}u_{l,jk} - D_i\varphi_k, \quad (115)$$

where H is the enthalpy of the system defined as

$$dH = T_{ij} dS_{ij} + \hat{T}_{ijk} dS_{jk,i} - D_i dE_i. \quad (116)$$

The J integral J_k is related to Q_{ik} through

$$J_k = \lim_{\varepsilon \rightarrow 0} \int_{\Gamma_\varepsilon} Q_{ik} n_i ds, \quad (117)$$

where Γ_ε is a closed contour around the crack tip whose outward normal is \mathbf{n} . The J integral is path independent, so any curve that includes the crack tip would yield the same result. But, we take $\varepsilon \rightarrow 0$ since we use an asymptotic solution which is only valid near the crack tip.

We are interested in J_1 , which is the energy release rate. It can be computed by using any closed contour around the crack tip. One such contour consists of an infinitesimally small closed circle that goes to the crack face, as shown in Fig. 4. Another one is the box contour as in Aravas and Giannakopoulos (2009), also shown in Fig. 4. Let us start with the circular contour for the Mode III crack. Using the constitutive relations, J_1^{III} has the following relation with w :

$$J_1^{\text{III}} = \frac{G}{2} \lim_{r \rightarrow 0} \int_{-\pi}^{\pi} \{ (w_{,2}^2 - w_{,1}^2) \cos \theta - 2w_{,1}w_{,2} \sin \theta + l_2^2 \left[\left(\nabla^2 w \right)^2 \cos \theta + 2w_{,1}(\nabla^2 w)_{,r} - 2w_{,1r} \nabla^2 w \right] \} r d\theta. \quad (118)$$

By substituting our asymptotic solution into the integral for J_1^{III} we find that

$$J_1^{\text{III}} = 2\pi\mu l_2^2 C_3^2 (1 - \alpha^2)(3 - 4\alpha^2) \geq \pi\mu l_2^2 C_3^2. \quad (119)$$

This is a positive quantity, exactly as in LEFM (Rice and Drucker, 1967). In what follows we show that the form of the energy release rate for Mode I and Mode II cracks in flexoelectric solids is similar to that in piezoelectric materials. The constant C_3 above is a function of the material constants and is related to the stress intensity K_{III} . In the limiting case of $\alpha, \beta, l \rightarrow 0$ we know that

$$\lim_{\alpha, \beta, l \rightarrow 0} J_1^{\text{III}} = \frac{K_{\text{III}}^2}{2\mu}. \quad (120)$$

Thus, if we remove all the SGE and flexoelectric effects from the material, the energy release rate converges to the results from linear elastic fracture mechanics. Now, for an infinite medium with a semi-infinite crack, we know that far away from the crack tip the fields should be the same as those of linear elasticity. Hence, by using the path independence of the J integral we can write

$$C_3 = \frac{K_{\text{III}}}{2\mu\sqrt{\pi l}} \left[(1 - \alpha^2)(3 - 4\alpha^2) \right]^{-1/2}. \quad (121)$$

In the case of $\alpha \rightarrow 0$, we get

$$C_3 = \frac{K_{III}}{2\mu\sqrt{3\pi l}}, \quad (122)$$

which recovers the result of Zhang et al. (1998) using couple stress theory, except that they used a length scale that is half of our's.

An alternative way of calculating J integral is to use the box contour as in Freund (1972). For planar cracks, this can be written as

$$J_1 = -2 \lim_{\epsilon \rightarrow 0} \int_{-\epsilon}^{\epsilon} \left[t_{12}u_{1,1} + t_{22}u_{2,1} + \hat{t}_{221}u_{1,12} + \hat{t}_{222}u_{2,12} + D_2\varphi_1 \right] \Big|_{x_2=0^+} dx_1. \quad (123)$$

For Mode I purely insulating (ID) and purely conducting (IE) conditions, the J-integrals are respectively given by

$$J_1^{ID} = \frac{\mu\pi l}{16(1-\nu)} \left[\frac{(5-4\nu) - (7-6\nu)\alpha^2}{1-\alpha^2} (3C_{11} - 2C_{12})^2 + 8C_{12}^2 \right], \quad (124)$$

$$J_1^{IE} = \mu\pi l \left[\frac{(5-4\nu) - (7-6\nu)\alpha^2}{16(1-\nu)(1-\alpha^2)} (3C_{11} - 2C_{12})^2 + \frac{1-\alpha^2 - (\alpha-\beta)^2(1-2\nu)}{1+(1-2\nu)(1-\beta^2)} C_{12}^2 \right]. \quad (125)$$

For Mode II purely insulating (IID) and purely conducting (IIE), they are respectively:

$$J_1^{IID} = \mu\pi l \left\{ \frac{4(1-\alpha^2)(1-\nu) \left[(5-4\nu) - (7-6\nu)\alpha^2 \right] C_{21}^2}{(2\alpha^2\nu - 3\alpha^2 + 1)^2} + \frac{C_{22}^2}{1-2\nu} \right\}. \quad (126)$$

$$J_1^{IIE} = \mu\pi l (1-\alpha^2) \left\{ \frac{4(1-\nu) \left[(5-4\nu) - (7-6\nu)\alpha^2 \right] C_{21}^2}{(2\alpha^2\nu - 3\alpha^2 + 1)^2} + \frac{1-\alpha^2 - (\alpha-\beta)^2(1-2\nu)}{(1-\alpha\beta)(1-2\nu)} C_{22}^2 \right\}. \quad (127)$$

The above expressions, in the limiting case of $\alpha, \beta \rightarrow 0$, reduce to the results of Aravas and Giannakopoulos (2009).

For Mode D:

$$J_1^D = -\frac{K_D^2}{2\epsilon} [1 - \alpha^2 - (1-2\nu)(\beta - \alpha)^2], \quad (128)$$

and for Mode E:

$$J_1^E = -\frac{\epsilon K_E^2}{2} [1 - \alpha^2 - (1-2\nu)(\beta - \alpha)^2]^{-1}. \quad (129)$$

For the mixed modes, Mode I & Mode E we have

$$J_1^{I\&E} = \frac{\mu\pi l}{16(1-\nu)} \left[\frac{(5-4\nu) - (7-6\nu)\alpha^2}{1-\alpha^2} (3C_{11} - 2C_{12})^2 + 8C_{12}^2 - 8(2-\beta^2-2\nu+2\beta^2\nu)(K_4^I)^2 \right], \quad (130)$$

and for Mode II & Mode D:

$$J_1^{II\&D} = \mu\pi l \left\{ \frac{4(1-\alpha^2)(1-\nu) \left[(5-4\nu) - (7-6\nu)\alpha^2 \right] C_{21}^2}{(2\alpha^2\nu - 3\alpha^2 + 1)^2} + \frac{(C_{22} - \alpha K_4^{II})^2}{1-2\nu} - (1-\alpha^2)(K_4^{II})^2 \right\}. \quad (131)$$

There are a few points that we note. First, unlike Mode III, the planar cracks have more intensity constants resulting from SGE, C_{11} , C_{12} or C_{21} , C_{22} . Just as in SGE cracks (Aravas and Giannakopoulos, 2009), these intensity factors are needed to characterize the fracture behavior. For example, C_{12} can be a good measure of the rotation intensity factor at the crack face. Second, in the mixed modes, flexoelectricity reduces the energy release rate compared to the SGE crack. We also note that the form of the above equations is similar to those for piezoelectric materials, where the electric intensity also reduces the energy release rate of a crack.

5.4. Fracture criterion

The present asymptotic analysis serves as a starting point for the study of crack propagation, but with some limitations. In our cases, the asymptotics is only valid within a region around the crack tip that is on the order of the flexoelectric length scale or the SGE length scale. We will apply some simple fracture criteria using the asymptotic solution.

As a well-known example, we recall the classical Griffith postulate regarding a critical energy release rate G_c for the crack to advance (Griffith, 1921):

$$J_1 = G_c. \quad (132)$$

With the equations for various J_1 on hand, it is possible to connect flexoelectric parameters at the crack tip to the far field

quantities that can be measured to calculate J_1 . For example, in the mixed Mode I & Mode E crack, we have $J_1 = f(C_{11}, C_{12}, K_4^I) = \tilde{f}(C_{11}, C_{12}, K_E)$, so fracture criteria of this type can be written as

$$\tilde{f}(C_{11}, C_{12}, K_E) - G_c = 0. \tag{133}$$

We recall the above criterion resembles that in piezoelectric materials (Schneider, 2007), except that the function \tilde{f} for piezoelectrics depends on only two constants, while for flexoelectric materials we have three. In both mixed modes, flexoelectricity tends to reduce the energy release rate. Hence, with the same G_c it requires more loading/energy to achieve the minimum condition for the crack to advance/grow if the material is flexoelectric versus when it is not.

Another important criterion for crack propagation depends on the crack opening displacement (COD). According to Aravas and Giannakopoulos (2009), the small-scale cohesive zone assumed by Barenblatt (1962) can be well modeled by the cusp-like curve of the COD produced by the SGE asymptotic analysis. Similarly, the flexoelectric COD criterion for crack propagation can be worked out as

$$\text{COD} \simeq 2u_1(l, \pi) = 2C_{11}l = \delta_c. \tag{134}$$

where δ_c is some critical crack opening displacement. In the above equation only C_{11} is explicitly involved. This is in contrast to the energy release rate criterion in which all three intensity factors are involved. Hence, measuring the COD could be a more practical way of determining the critical condition for crack growth. Recall that the critical opening for propagation of the crack is δ_c which is a material property. As mentioned in Aravas and Giannakopoulos (2009), the critical value C_{11c} could serve as the measure which determines when crack growth occurs without assuming the length of the cohesive zone. The parameter C_{11} in SGE can be calculated through finite element simulation of a finite crack. We expect to do this in the near future for a flexoelectric solid. But, in order to illustrate the applicability of this idea to flexoelectric materials we adopt a data set obtained from Tsantidis and Aravas (2011) as a zero order approximation and hold the loading/energy release rate fixed. We want to see how C_{11} changes if we change K_E . This is shown in Fig. 5. From this figure it is apparent that for larger K_E we need to supply more energy in order to achieve the critical COD at a given r and cause the crack to grow.

Lastly, a flexoelectric material is a dielectric, therefore failure also arises from the electric properties of the material. For example, since K_E or K_D is itself a measurable quantity, a simple failure condition could be

$$K_E = K_{Ec} \tag{135}$$

where K_{Ec} is a critical intensity factor for the electric field (governed, for example, by the condition for electric breakdown).

Since the electric displacement field is singular near the crack tip we can expect some non-linearity to overwhelm the linear constitutive laws much like the plastic zone in small-scale yielding. As advocated by Gao et al. (1997), a simple non-linear model of ferroelectric solids behaves like an elastic–perfectly plastic material where the stress stays the same irrespective of strain after reaching a yield stress. For the simple non-linear ferroelectric (Gao et al., 1997) the electric displacement stays the same irrespective of the strain. Just like the plastic zone in small-scale yielding we will have a zone around the crack in a flexoelectric solid in which the electric displacement is a constant, so that

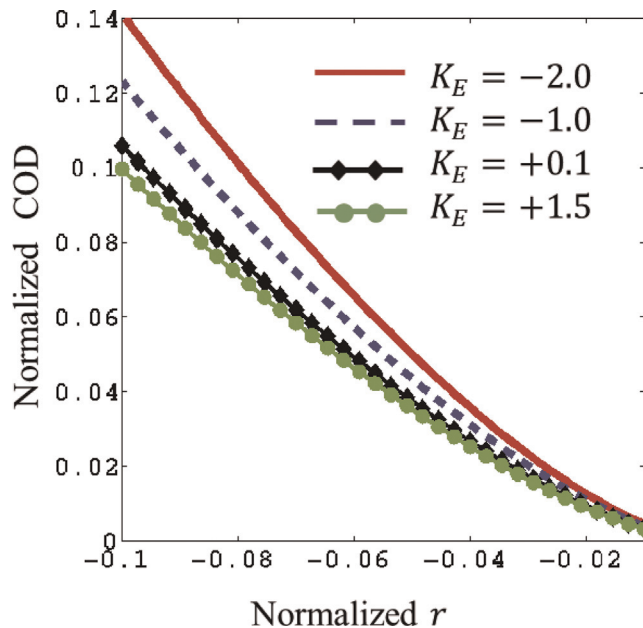


Fig. 5. The COD profile of mixed Mode I & Mode E cracks with different values of K_E . The energy release rate is held fixed. The COD and r are both normalized against the SGE length scale l . K_E is normalized against $\sqrt{2\pi l|c}$.

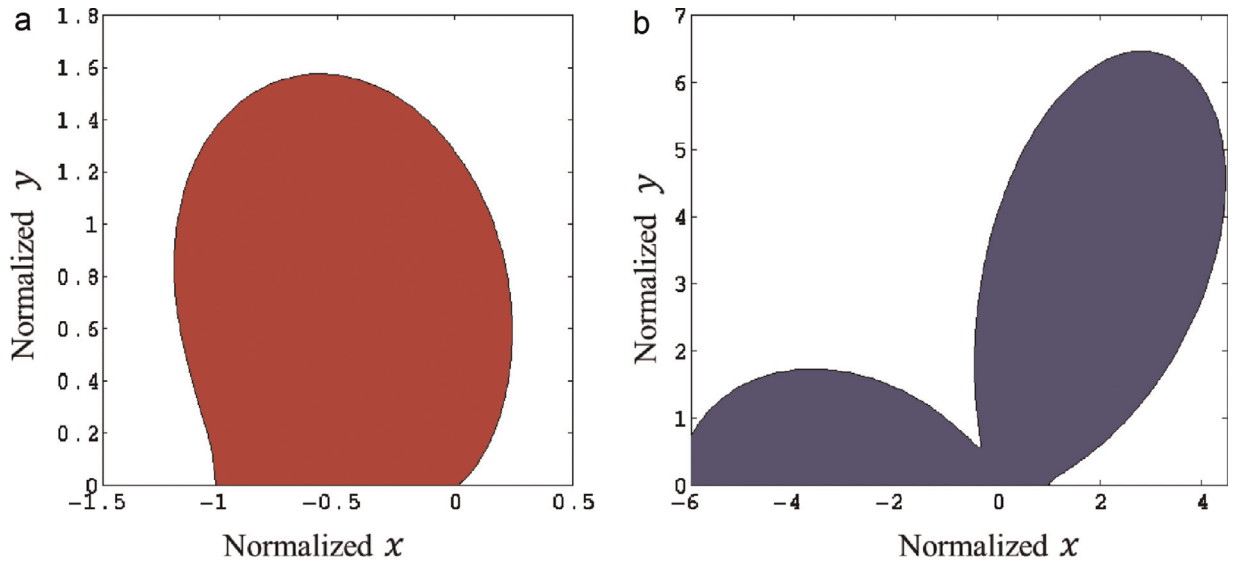


Fig. 6. Electric yielded zone near crack tips. (a) Mode I & Mode E crack, (b) Mode II & Mode D crack. In both cases, $\bar{D}_Y = 1.0$ and the crack tip is located at $x=0$. All material constants are the same as those in Figs. 3 and 5. Notice the similarity of the shape of the electric yielded zone with that of the plastic yielded zone for these cracks.

$$\sqrt{\frac{D_1^2 + D_2^2}{\mu\epsilon}} = \bar{D}_Y, \quad (136)$$

where \bar{D}_Y is a non-dimensional yielding electric displacement parameter. Electric yielding of this type has been studied in piezoelectricity (Gao et al., 1997; Wang, 2000; Schneider, 2007; Kuna, 2010). Similar to the plastic zone in elasticity, this phenomenon protects the material from singularities in the presence of a crack. The electric yielded zones of mixed modes cracks are shown in Fig. 6. These zones are associated with phase transition and domain switching (Gao et al., 1997; Wang, 2000), an analysis of which is beyond the scope of this work.

6. Conclusions

In this paper we have analyzed the stress and polarization fields near point defects, dislocations and cracks in flexoelectric solids. We have shown that flexoelectricity plays an important role in the immediate vicinity of these defects where there are large strain gradients. We have tried to connect our analysis to experiments wherever possible and have also given predictions that can be tested. The most interesting of these connections is to experiments on electromechanical phenomena in ice. The electrical behavior of defects in ice had been explained earlier by a “pseudo-piezoelectricity”, which we now recognize as flexoelectricity. The latter half of the paper is devoted to asymptotic solutions for crack tip fields in flexoelectric solids. While there is a wealth of literature on cracks in piezoelectrics, little is known about cracks in flexoelectric materials. Our’s is a first attempt to learn something about the nature of singularities near cracks in flexoelectric solids. The usual $r^{1/2}$ singularity of the displacement in both LEFM and LPFM is replaced by higher order $r^{3/2}$ singularity due to gradient effects. Gradient effects also introduce new intensity factors which could not be computed in our analysis but may be amenable to computation using finite elements. By employing the J integral, we found that, similar to piezoelectric solids, electric coupling reduces the energy release rate so that more energy must be supplied in order for a crack to grow.

Acknowledgment

We acknowledge support for this work through the Army Research Office Grant no. W911NF-11-1-0494. We thank Prof. Nikolaos Aravas for insightful discussions.

Appendix A

A.1. Conventional intensity factors

Mode III cracks in flexoelectric solids are very similar to those in SGE and they inherit the same intensity factors (Zhang

et al., 1998). We will focus here on the planar cracks. Due to strain gradient and electrostatics we now have more intensity factors to calculate. Unfortunately, if we use the conventional intensity factors K_I , K_{II} , K_{IV} and K_E then the expressions for the energy release rate become too cumbersome. We could use the definitions for intensity factors as in Aravas and Giannakopoulos (2009), but C_{ij} , $i, j = 1, 2$, and $K_4^{I,II}$ give us a more compact way of presenting the major results. In the following we will connect these constants to the conventional intensity factors.

For stresses, we follow Aravas (2011) and write

$$\sigma_{ij} = T_{ij} - \frac{2}{3}\hat{T}_{ijk,k} - \frac{1}{3}\hat{T}_{kij,k} \tag{A.1}$$

The stress defined in this manner is called the true stress (Mindlin and Eshel, 1968) and is consistent with couple-stress theory. Now, for the conventional K_I intensity we need σ_{22} at $\theta = 0$. The dominant term for σ_{22} is

$$\begin{aligned} \sigma_{22}(r, 0) = & -\frac{\mu(r/l)^{-3/2}}{12(1-\nu)(1-\alpha^2)} \{3C_{11}(1+\alpha\beta-3\alpha^2)(1-\nu) + 2C_{12}[\alpha(\beta+2\alpha)(1-\nu) + \nu(1-\alpha^2)] \\ & + 2K_4^I(1-\alpha^2) \left[\beta(1-2\nu) - \alpha(1-\nu) \right] \}. \end{aligned} \tag{A.2}$$

The K_I intensity factor is defined as

$$K_I = \lim_{r \rightarrow 0} \sqrt{2\pi r} \sigma_{22}(r, 0) \rightarrow \infty. \tag{A.3}$$

We have found that the conventional definition of K_I is not useful here just as in SGE (Aravas and Giannakopoulos, 2009). The reason for this is that the stress is singular as $r^{-3/2}$ due to strain gradient effects. Hence, we define

$$\begin{aligned} K_I = \lim_{r \rightarrow 0} \sqrt{\frac{2\pi r^3}{l^2}} \sigma_{22}(r, 0) = & -\frac{\mu\sqrt{2\pi l}}{12(1-\nu)(1-\alpha^2)} \{3C_{11}(1+\alpha\beta-3\alpha^2)(1-\nu) \\ & + 2C_{12} \left[\alpha(\beta+2\alpha)(1-\nu) + \nu(1-\alpha^2) \right] + 2K_4^I(1-\alpha^2) \left[\beta(1-2\nu) - \alpha(1-\nu) \right] \} \end{aligned} \tag{A.4}$$

Similarly, we can define the following K_{II} in mode II:

$$K_{II} = \lim_{r \rightarrow 0} \sqrt{\frac{2\pi r^3}{l^2}} \sigma_{12}(r, 0). \tag{A.5}$$

We find that

$$\begin{aligned} K_{II} = & \frac{\mu\sqrt{2\pi l}}{12(1-2\nu)(2\alpha^2\nu-3\alpha^2+1)} \{64\beta K_4^{II}\alpha^2\nu - 24\beta K_4^{II}\alpha^2 - 16\beta K_4^{II}\nu + 16C_{22}\alpha^2\nu - 56\alpha^3\nu K_4^{II} \\ & + 10\alpha K_4^{II}\nu + 20\alpha^3\nu^2 K_4^{II} - 25C_{21} - 72\alpha^2\nu C_{21} + 36\alpha^2\nu^2 C_{21} + 8\beta K_4^{II} - 32C_{21}\nu^2 + 39\alpha^3 K_4^{II} \\ & - 13\alpha K_4^{II} - 24\alpha^2 C_{22} - 32\beta K_4^{II}\alpha^2\nu^2 + 27\alpha^2 C_{21} + 66C_{21}\nu + 8C_{22}\}. \end{aligned} \tag{A.6}$$

For the electric intensities

$$K_E = \lim_{r \rightarrow 0} \sqrt{2\pi r} E_1(r, 0) = \sqrt{\frac{2\pi\mu l}{\epsilon}} \left[\alpha C_{12} - K_4^I + \frac{1-2\nu}{2-2\nu} \left(\beta^2 K_4^I - \beta C_{12} \right) \right] \tag{A.7}$$

$$K_{IV} = \lim_{r \rightarrow 0} \sqrt{2\pi r} D_2(r, 0) = \sqrt{2\pi\mu\epsilon l} K_4^{II} \tag{A.8}$$

A.2. Bounds for f_1 and f_2

The energy storage function W is positive definite as a requirement for uniqueness of BVP solutions. Let $W^R = W - SE$ where SE is the strain energy, whose positive-definiteness is imposed by classic elasticity:

$$3\lambda + 2\mu > 0, \quad \mu > 0. \tag{A.9}$$

Since flexoelectricity only has to do with the gradient terms and electric terms, bounds for them should be derived from W^R . Now, rewrite W^R as

$$W^R = \frac{1}{2}(3\lambda + 2\mu)l^2\theta_{,i}\theta_{,i} + (3f_1 + 2f_2)\theta_{,i}P_i + \mu l^2 S'_{ij,j}S'_{ik,k} + 2f_2 S'_{ik,k}P_i + \frac{1}{2}aP_i^2, \quad (\text{A.10})$$

where S'_{ij} is the deviatoric strain tensor and θ and S'_{ij} are independent of each other. Hence, we could suppose that $S'_{jk,i} = 0$ but P_i and $\theta_{,i}$ are not. Then, to retain the positive definiteness of the above equation, the minimum of W^R has to satisfy the following constraint:

$$\min\{W^R, S'_{jk,i} = 0\} = \frac{1}{2}\left[a - \frac{(3f_1 + 2f_2)^2}{(3\lambda + 2\mu)l^2}\right]P_iP_i \geq 0. \quad (\text{A.11})$$

The above inequality gives the bounds for the constant $|3f_1 + 2f_2|$:

$$|3f_1 + 2f_2| \leq l\sqrt{(3\lambda + 2\mu)a}. \quad (\text{A.12})$$

The same procedure could be used for $S'_{jk,i}$, $P_i \neq 0$ and $\theta = 0$ to give

$$|f_2| \leq l\sqrt{\frac{\mu a}{2}}. \quad (\text{A.13})$$

Therefore, in general, the thermodynamic constraints for the flexoelectric constants are

$$|3f_1 + 2f_2| \leq l\sqrt{(3\lambda + 2\mu)a}, \quad |f_2| \leq l\sqrt{\frac{\mu a}{2}}. \quad (\text{A.14})$$

If we were to convert this to non-dimensionalized parameters α, β as defined in the crack mechanics section, and Poisson's ratio ν , we get

$$|3\beta - 2\alpha| \leq \frac{2(1 + \nu)}{1 - 2\nu}, \quad |\alpha| \leq \sqrt{\frac{1}{2}}. \quad (\text{A.15})$$

References

- Abdollahi, A., Peco, C., Milln, D., Arroyo, M., Arias, I., 2014. Computational evaluation of the flexoelectric effect in dielectric solids. *J. Appl. Phys.* 116 (9).
- Adler, W.F., 1969. Point-defect interactions in elastic materials of grade 2. *Phys. Rev.* 186 (3), 666.
- Aravas, N., 2011. Plane-strain problems for a class of gradient elasticity models—a stress function approach. *J. Elast.* 104, 45–70.
- Aravas, N., Giannakopoulos, A., 2009. Plane asymptotic crack-tip solutions in gradient elasticity. *Int. J. Solids Struct.* 46 (25), 4478–4503.
- Barenblatt, G.I., 1962. The mathematical theory of equilibrium cracks in brittle fracture. *Adv. Appl. Mech.* 7 (1), 55–129.
- Buka, A., Eber, N., 2012. Flexoelectricity in Liquid Crystals: Theory, Experiments and Applications. Imperial College Press, London.
- Catalan, G., Lubk, A., Vlooswijk, A.H.G., Snoeck, E., Magen, C., Janssens, A., Rispen, G., Rijnders, G., Blank, D.H.A., Noheda, B., 2011. Flexoelectric rotation of polarization in ferroelectric thin films. *Nat. Mater.* 10 (December), 963–967.
- Chin, H.-A., Mao, S., Huang, C.-T., Ohemeng, K.K., Wagner, S., Purohit, P.K., McAlpine, M.C., 2015. Pyro-paraelectricity. *Extreme Mech. Lett.* 2, 20–27, ISSN 2352-4316, <http://dx.doi.org/10.1016/j.eml.2014.12.009>.
- Eringen, A.C., 1984. Theory of nonlocal piezoelectricity. *J. Math. Phys.* 25 (3), 717–727.
- Eshelby, J., 1966. A simple derivation of the elastic field of an edge dislocation. *Br. J. Appl. Phys.* 17 (9), 1131.
- Evtushenko, A., Maeno, N., Petrenko, V., Ryzhkin, I., 1987. Pseudopiezoelectric effects in ice. *Le J. Phys. Colloq.* 48 (C1), C1–109.
- Freund, L., 1972. Energy flux into the tip of an extending crack in an elastic solid. *J. Elast.* 2 (4), 341–349.
- Gao, H., Zhang, T.-Y., Tong, P., 1997. Local and global energy release rates for an electrically yielded crack in a piezoelectric ceramic. *J. Mech. Phys. Solids* 45 (4), 491–510.
- Griffith, A.A., 1921. The phenomena of rupture and flow in solids. *Philos. Trans. R. Soc. Lond. Ser. A*, 163–198.
- Harden, J., Chambers, M., Verduzco, R., Luchette, P., Gleeson, J.T., Sprunt, S., Jáklí, A., 2010. Giant flexoelectricity in bent-core nematic liquid crystal elastomers. *Appl. Phys. Lett.* 96 (10), 102907.
- Hobbs, M.E., Jhon, M.S., Eyring, H., 1966. The dielectric constant of liquid water and various forms of ice according to significant structure theory. *Proc. Natl. Acad. Sci. USA* 56 (1), 31.
- Hong, J., Vanderbilt, D., 2011. First-principles theory of frozen-ion flexoelectricity. *Phys. Rev. B* 84, 180101.
- Hong, J., Vanderbilt, D., 2013. First-principles theory and calculation of flexoelectricity. *Phys. Rev. B* 88, 174107.
- Koehler, J.S., Langreth, D., von-Turkovich, B., 1962. Charged dislocations in ionic crystals. *Phys. Rev.* 128 (Oct), 573–580.
- Kuna, M., 2010. Fracture mechanics of piezoelectric materials—Where are we right now? *Eng. Fract. Mech.* 77 (2), 309–326.
- Lazar, M., 2013. The fundamentals of non-singular dislocations in the theory of gradient elasticity: dislocation loops and straight dislocations. *Int. J. Solids Struct.* 50 (2), 352–362.
- Lazar, M., Maugin, G.A., 2006. Dislocations in gradient elasticity revisited. *Proc. R. Soc. A: Math. Phys. Eng. Sci.* 462 (2075), 3465–3480.
- Ma, W., Cross, L.E., 2001. Large flexoelectric polarization in ceramic lead magnesium niobate. *Appl. Phys. Lett.* 79, 4420–4422.
- Ma, W., Cross, L.E., 2002. Flexoelectric polarization of barium strontium titanate in the paraelectric state. *Appl. Phys. Lett.* 81, 3440–3442.
- Mao, S., Purohit, P.K., 2014. Insights into flexoelectric solids from strain-gradient elasticity. *J. Appl. Mech.* 81 (8), 081004.
- Maranganti, R., Sharma, P., 2007. A novel atomistic approach to determine strain-gradient elasticity constants: tabulation and comparison for various metals, semiconductors, silica, polymers and the (ir) relevance for nanotechnologies. *J. Mech. Phys. Solids* 55 (9), 1823–1852.
- Maranganti, R., Sharma, P., 2009. Atomistic determination of flexoelectric properties of crystalline dielectrics. *Phys. Rev. B* 80, 054109.
- Meyer, R.B., 1969. Piezoelectric effects in liquid crystals. *Phys. Rev. Lett.* 22 (May), 918–921.
- Mindlin, R.D., Eshel, N.N., 1968. On first strain-gradient theories in linear elasticity. *Int. J. Solids Struct.* 4, 637–642.
- Nguyen, T.D., Mao, S., Yeh, Y.-W., Purohit, P.K., McAlpine, M.C., 2013. Nanoscale flexoelectricity. *Adv. Mater.* 25, 946–974.
- Nowacki, J.P., 2006. *Static and Dynamic Coupled Fields in Bodies with Piezoeffects or Polarization Gradient*. Springer Verlag, Berlin, Heidelberg, New York.

- Pak, Y., 1992. Linear electro-elastic fracture mechanics of piezoelectric materials. *Int. J. Fract.* 54 (1), 79–100.
- Petrenko, V., Whitworth, R., 1983. Electric currents associated with dislocation motion in ice. *J. Phys. Chem.* 87 (21), 4022–4024.
- Petrenko, V.F., 1996. *Electromechanical Phenomena in Ice*. Technical Report. DTIC Document.
- Petrenko, V.F., Whitworth, R.W., 1999. *Physics of Ice*. Oxford University Press, New York.
- Petrov, A.G., 2006. Electricity and mechanics of biomembrane systems: flexoelectricity in living membranes. *Anal. Chim. Acta* 568, 70–83.
- Phillips, R., 2001. *Crystals, Defects and Microstructures: Modeling Across Scales*. Cambridge University Press, Cambridge.
- Raphael, R.M., Popel, A.S., Brownell, W.E., 2010. A membrane bending model of outer hair cell electromotility. *Biophys. J.* 78, 2844–2862.
- Rice, J., Drucker, D.C., 1967. Energy changes in stressed bodies due to void and crack growth. *Int. J. Fract. Mech.* 3 (1), 19–27.
- Schneider, G.A., 2007. Influence of electric field and mechanical stresses on the fracture of ferroelectrics. *Mater. Res.* 37 (1), 491.
- Sharma, P., Ganti, S., 2005. Gauge-field-theory solution of the elastic state of a screw dislocation in a dispersive (non-local) crystalline solid. *Proc. R. Soc. A: Math. Phys. Eng. Sci.* 461 (2056), 1081–1095.
- Sosa, H., 1992. On the fracture mechanics of piezoelectric solids. *Int. J. Solids Struct.* 29 (21), 2613–2622.
- Suo, Z., Kuo, C.-M., Barnett, D., Willis, J., 1992. Fracture mechanics for piezoelectric ceramics. *J. Mech. Phys. Solids* 40 (4), 739–765.
- Tsantidis, G., Aravas, N., 2011. Cracked-panel solution in gradient elasticity. *ICEAF II*.
- Turchányi, G., Mátrai, M., Janszky, J., Tarján, I., 1973. Experimental study on the electric field of dislocations in coloured alkali halide crystals. *J. Phys. Colloq.* 34, C9-261–C9-264.
- Wang, T., 2000. Analysis of strip electric saturation model of crack problem in piezoelectric materials. *Int. J. Solids Struct.* 37 (42), 6031–6049.
- Whitworth, R., 1975. Charged dislocations in ionic crystals. *Adv. Phys.* 24 (2), 203–304.
- Yang, J., 2005. *An Introduction to the Theory of Piezoelectricity*. Springer, New York.
- Zelisko, M., Hanlumuang, Y., Yang, S., Liu, Y., Lei, C., Li, J., Ajayan, P.M., Sharma, P., 2014. Anomalous piezoelectricity in two-dimensional graphene nitride nanosheets. *Nat. Commun.* 5.
- Zhang, L., Huang, Y., Chen, J., Hwang, K., 1998. The mode iii full-field solution in elastic materials with strain gradient effects. *Int. J. Fract.* 92 (4), 325–348.
- Zubko, P., Catalan, G., Buckley, A., Welche, P.R.L., Scott, J.F., 2007. Strain-gradient-induced polarization in SrTiO₃ single crystals. *Phys. Rev. Lett.* 99, 167601.
- Zubko, P., Catalan, G., Tagantsev, A.K., 2013. Flexoelectric effect in solids. *Annu. Rev. Mater. Res.* 43 (1), 387–421.